Electronic Structure and Properties of High-Tc Superconductor Y-Ba-Cu-O. 1. Oxygen-deficiency in the $YBa_2Cu_3O_x$ Superconductor ($6 \leq x \leq 7$)

U-Hyon Paek*

Department of Chemistry, Gyeongsang National University, Jinju 660-701

U-Sung Choi and Kee-Hag Lee†

Department of Chemistry, Wonkwang University, Iri 570-749

Chang-Hong Kim

Inorganic Chemistry Laboratory, Korea Advanced Institute of Science and Technology, Seoul 130-650.
Received July 4, 1989.

The effect of oxygen-deficiency on the charge distributions and orbital energies for small copper oxide clusters representing the superconducting materials $YBa_2Cu_3O_x$ ($6 \leq x \leq 7$) were investigated by the extended Hückel molecular orbital (EHMO) method with the tight-binding model. Our calculations show +3 oxidation state of Cu(1) in the CuO_3 chain and +2 or +1 of Cu(2) in the CuO_2 layers for $YBa_2Cu_3O_7$ with the nominal charge of $Cu_3 = +7$ (or +5), while for $YBa_2Cu_3O_6$ +1 oxidation state of Cu(1) and +3 (or +2) of Cu(2) in the CuO_2 layers with the nominal charge of $Cu_3 = +7$ (or +5). For Cu_3O_{12} cluster representing $YBa_2Cu_3O_7$ with the nominal charge of $Cu_3 = +7$ the Cu(2) $d_{x^2-y^2}$ orbitals in the CuO_2 layers is a typical Jahn-Teller d^9 system with the partial hole and the Cu(1) d_{z2-y2} orbital in the CuO_3 chain contains hole occupancy. For Cu_3O_{10} cluster representing $YBa_2Cu_3O_6$ with the nominal charge of Cu = +5 the orbital character of the highest partially occupied MO (HPOMO) and the lowest completely unoccupied MO (LCUMO) of Cu_3O_{12} representing $YBa_2Cu_3O_7$ with the nominal charge of $Cu_3 = +7$ is reversed, and the character of Cu(1) $d_{x^2-y^2}$ orbital of LCUMO of the Cu_3O_{12} cluster is vanished. It is suggested that the local crystal field environment of Cu(1) by the oxygens in the Cu(1) chain may play a vital role in conductivity and superconductivity, either alone or through cooperative electronic coupling with the Cu(2) layers in $YBa_2Cu_3O_7$.

Introduction

The discovery of oxide superconductors with Tc's as high as 94K has raised questions concerning the mechanism of superconductivity in these materials. The nature of electron states in these materials plays a key role in understanding the properties and the possible superconductivity mechanism in these complex ceramic oxides. .

The phase in the Y-Ba-Cu-O system responsible for superconductivity[1] in the 90K range has been identified as $YBa_2Cu_3O_x$ and its structure has been determined by X-ray and neutron diffractions.[2] Valence fluctuations of copper oxide clusters representing the new superconducting materials $YBa_2Cu_3O_{7-y}$ have been calculated by semiempirical molecular orbital (EHMO) methods,[3] and the tight-binding band electronic structure of the stoichiometric composition $YBa_2Cu_3O_{7-y}$ is calculated on the basis of its crystal structure determined by Beno *et al.*[4,5] The $YBa_2Cu_3O_x$ system exhibits tetragonal-to-orthorhombic structural phase transitions which are associated with the ordering of oxygen vacancies in the local plane or the change of temperature.[6a,6b]

In samples showing the highest values of Tc, the oxygen stoichiometry is slightly less than 7, and the crystal structure is orthorhombic (see Figure 1(a)).[7]

The Cu(1) atoms form CuO_3 chains along the *b* axis, and the Cu(2) atoms form dimpled CuO_2 layers in the *ab* plane.[2] The Cu(2) atoms are out of O(2)-O(3) plane toward the side facing the Ba^{2+} cation. Each Cu(2) atom of the CuO_2 layers is capped by the oxygen O(4) of the CuO_3 chains, there by leading a square-pyramidal coordination for Cu(2).

Each Y^{3+} cation has a square-prismatic coordination provided by two sandwiching CuO_2 layers, while each Ba^{2+} cation is located in an oxygen pocket made of four oxygen atoms of a CuO_2 layer and six oxygen atoms of two CuO_3 chains. In turn, the Y^{3+} and Ba^{2+} cations form $(Y^{3+}-Ba^{2+}-Ba^{2+}-)_\infty$ chains along the *c* axis. The crystal structure of $YBa_2Cu_3O_6$ is derived from the $YBa_2Cu_3O_7$ structure. Namely, the oxygen is removed from the O(1) site in the $YBa_2Cu_3O_7$ structure,[7] leaving Cu(1) in two-fold coordinations. This structure is consistent with the results of Beech *et al.*[7,8a] and orthorhomic $YBa_2Cu_3O_{7-y}$ ($y < 0.5$) undergoes a phase transition to a tetragonal structure as *y* increases beyond ~0.5 upon increasing temperature.[8b] Particularly, the orthorhombic phase gives metallic behavior and a sharp superconducting transition near 90K and the two different samples of the tetragonal phase give semiconducting behaviors for one sample and mixed metallic-semiconductive behaviors for another which exhibits a broad superconducting transition near 60K.[8c]

More interestingly, occurence of superconductivity with $6 \leq x \leq 7$ (especially $x \simeq 6.5$) is better explained by intergrowths of "O_7" domains and insulating "O_6" domains by electron microscopic observations (see Figure 4).[8d,e,4]

From the above description, we think the oxygen holds the key to determine the superconductivity. It is interesting to compare the electronic structure of $YBa_2Cu_3O_x$ with $x = 6$

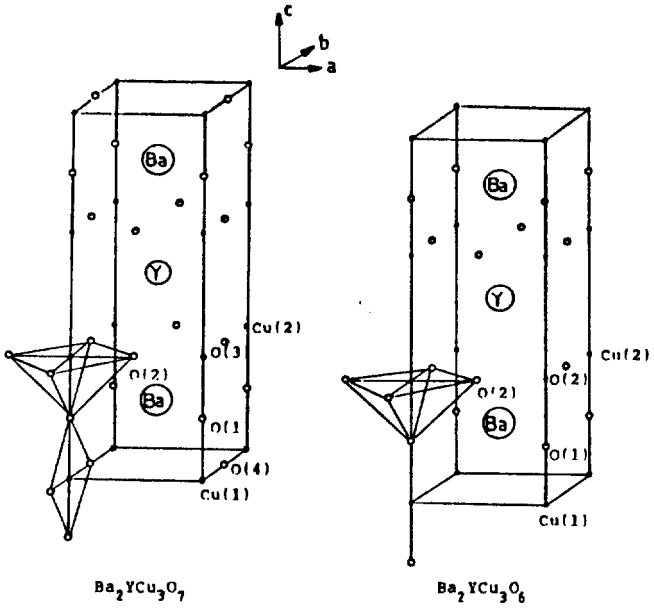

Figure 1. Schematic unit cells for $YBa_2Cu_3O_x$ ($6 \le x \le 7$).

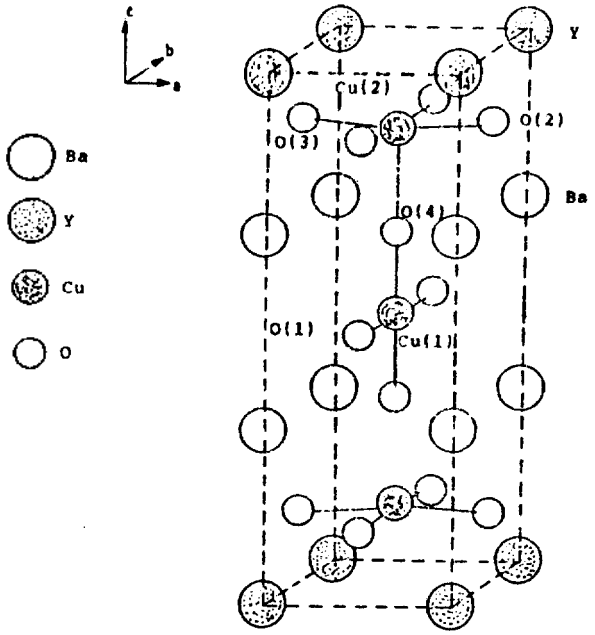

Figure 2. Crystal structure of orthorhombic $YBa_2Cu_3O_7$ (ordered vacancy model). In $YBa_2Cu_3O_6$, the O(1) site is vacant.

and $x = 7$ using valence description of the molecular crystals.

The purpose of present work is to understand the effect of the oxygen-deficiency on the electronic structure and properties of the $YBa_2Cu_3O_x$ superconductor ($6 \le x \le 7$).

The calculations were of the extended Hückel method with the tight-binding model.

Investigation of Electronic Structure and Properties

Schematic unit cells for $YBa_2Cu_3O_x$ are in Figure 1.[7,8a,9,10] Shown in Figure 2 is possible crystal structures for $YBa_2Cu_3O_x$ ($6 \le x \le 7$).[8,8a,9,10,13] The hypothetical clusters[14] shown in Figure 3 is taken to be our models for calculations

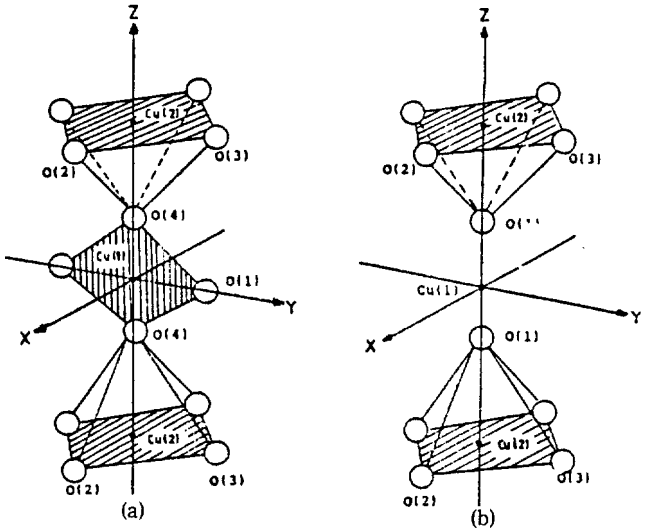

Figure 3. (a) Local environment for the Cu(1) and Cu(2) atoms in $YBa_2Cu_3O_7$. (b) Local environment for the Cu(1) and Cu(2) atoms in $YBa_2Cu_3O_6$.

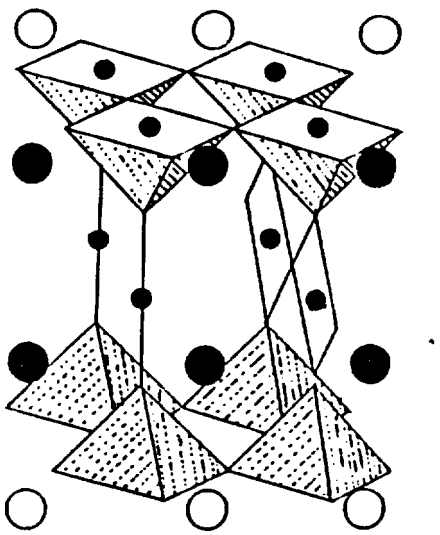

Figure 4. Intergrowths of superconducting "O_7" domains (CuO_4 square-planar groups) and insulating "O_6" domains (Cu in 2-fold coordination).

of $YBa_2Cu_3O_7$ and $YBa_2Cu_3O_6$ cuprates in Figures 1 and 2. The Y and Ba cations are not included as the Y cations separate the two sets of CuO_2 layers and the Ba cations form Ba–O(4) planes that should not effect the energy levels of the CuO_3 chain and the CuO_2 layers significantly. Massida *et al.*[14] have noted that the Y and Ba atoms form an ordered superlattice structure and it is the O vacancies which appear to play an important role in stabilizing the new superconductor, $YBa_2Cu_3O_{7-y}$.

The Cu_3O_{12} cluster with a charge of each of (-17) and (-15) represents $YBa_2Cu_3O_7$ with no vacancies and the Cu_3O_{10} cluster each of (-13) and (-15) is used in $YBa_2Cu_3O_6$ with O(1) vacancies when we take the nominal charge of $Cu_3 = +7$ and $+5$. Shown in Figure 4 is intergrowths of superconducting "O_7" domains (CuO_4 square-plannar groups) and insulating "O_6" domains (Cu in 2-fold coordina-

Table 1. Atomic Coordinates of $YBa_2Cu_3O_7$ and $YBa_2Cu_3O_6$

Atom	*X/a*	*Y/b*	*Z/c*[a] $YBa_2Cu_3O_7$	*Z/c*[b] $YBa_2Cu_3O_6$
Ba	0.50	0.50	0.1843	0.1952
Y	0.50	0.50	0.50	0.50
Cu(1)	0.00	0.00	0.00	0.00
Cu(2)	0.00	0.00	0.3556	0.3607
O(1)	0.00	0.50	0.00	vacancy
O(2)	0.50	0.00	0.3773	0.3791
O(3)	0.00	0.50	0.3789	0.3791
O(4)	0.00	0.00	0.1584	0.1518

[a]Beno *et al.*[5], (Argonne): $YBa_2Cu_3O_7$: $a = 3.8231$, $b = 3.8863$, $c = 11.6807$ Å. [b]Santoro *et al.*[8a], (National Bureau of Standards and At & T Bell): $YBa_2Cu_3O_6$: $a = b = 3.8570$, $c = 11.8194$ Å.

Table 2. Extended Hückel Parameters for Valence Orbitals[15]

	H_{11} (eV)			Exponents		
	s	*p*	*d*	*s*	*p*	*d*
Cu	-11.4	-6.06	-14.0	2.2	2.2	5.95(0.5933)
O	-32.3	-14.8		2.275	2.275	2.30(0.5744)

Table 3. Energy Gaps between Cu(1) $d_{z^2-y^2}$ State and Cu(2) $d_{x^2-y^2}$ State, Total Energies, and Relative Stabilities in Cu_3O_{12} and Cu_3O_{10} Clusters

	ΔE[E(Cu(1)$d_{z^2-y^2}$) -E(Cu(2)$d_{x^2-y^2}$)][a]	Total energy[b]	Relative Stability[c]	
$Cu_3O_{12}^{17-}$	0.388	-2215.387	(0)	
$Cu_3O_{12}^{19-}$	0.388	-2239.095	4.292	
$Cu_3O_{10}^{13-}$	1.499	-1909.942	57.847	(0)
$Cu_3O_{10}^{15-}$	1.499	-1933.554	62.233	(4.388)

[a]For $Cu_3O_{10}^{n-}$, *y*-directions of $d_{z^2-y^2}$ become lost. [b]For the total energy: just associated with the valence electron without the inner or nonvalence electrons. [c]For the relative stability: $= \varepsilon_{to}[Cu_3O_z^{n-}] - \{(12-z)\varepsilon_o - m(\text{VSIP of Cu } d\text{-state})\} - \varepsilon_{to}[Cu_3O_{12}^{17-}]$, where $z = 10, 12$; $n = 13, 15, 17, 19$; $m = 0, 2$; and ε_o is the sum of the VSIP of the neutral O atoms, respectively.

tion).

We have used the extended Hückel molecular orbital (EHMO) theory with the tight-binding model in calculations on the electron structures of copper-oxide clusters representing Y-Ba-Cu-O High Tc superconducting materials.

For orthorhombic $YBa_2Cu_3O_7$ and tetragonal $YBa_2Cu_3O_6$, we use the atomic coordinates obtained by Beno *et al.*[5] and Santoro *et al.*[8a], using neutron scattering technique, as shown in Table 1.

Table 2 represents extended Hückel parameters for the valence orbitals of EHMO calculations with the tight-binding model on Cu_3O_{12} and Cu_3O_{10} clusters representing $YBa_2Cu_3O_7$ and $YBa_2Cu_3O_6$ cuprates.

Here we choose the nominal charges of each ions as follows: +7 and +5 for Cu_3 ions; +3 for Y ions; +2 for Ba ions; -2 for O ions.

The energy gaps between Cu(1) $d_{z^2-y^2}$ state and Cu(2) $d_{x^2-y^2}$ state, total energies, and relative stabilities on Cu_3O_{12} and Cu_3O_{10} clusters representing $YBa_2Cu_3O_7$ and $YBa_2Cu_3O_6$ cuprates are shown in Table 3.

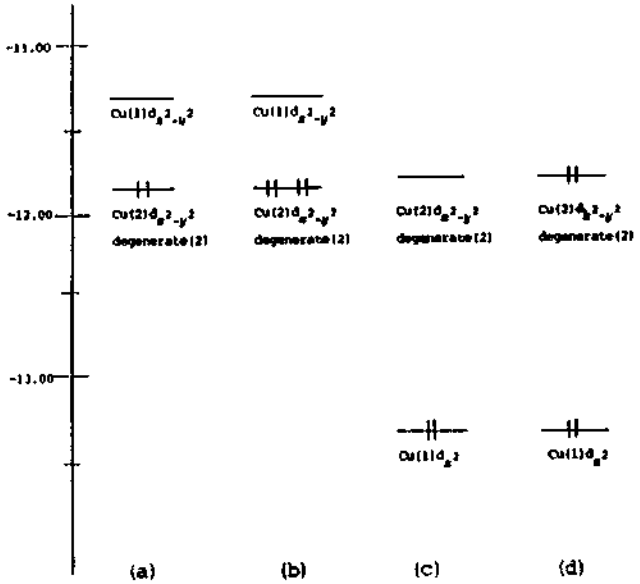

Figure 5. Molecular energy (eV) levels and electron configurations: (a) $Cu_3O_{12}^{17-}$; (b) $Cu_3O_{12}^{19-}$; (c) $Cu_3O_{10}^{13-}$; (d) $Cu_3O_{10}^{15-}$ clusters.

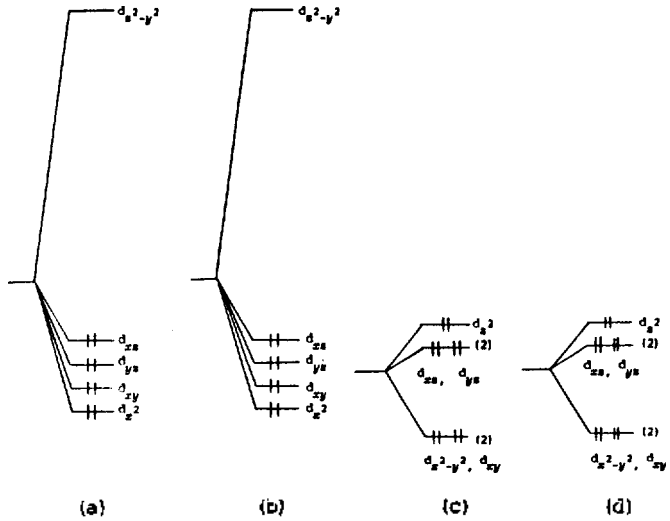

Figure 6-1. The splitting of the *d*-orbitals of Cu(1) by the local crystal field environment: (a) $Cu_3O_{12}^{17-}$; (b) $Cu_3O_{12}^{19-}$; (c) $Cu_3O_{10}^{13-}$; (d) $Cu_3O_{10}^{15-}$ clusters.

The important energy levels for Cu_3O_{12} and Cu_3O_{10} clusters representing $YBa_2Cu_3O_7$ and $YBa_2Cu_3O_6$ cuprates are illustrated in Figure 5.

Shown in Figure 6-1 and Figure 6-2 are another instructive splitting diagrams of each Cu *d*-orbitals in the clusters representing $YBa_2Cu_3O_7$ and $YBa_2Cu_3O_6$.

The computed *s,p,d* valence populations for each Cu and O ions are shown in Table 4. Shown in Table 5 are reduced overlap populations in Cu_3O_{12} and Cu_3O_{10} clusters representing $YB_2Cu_3O_7$ and $YBa_2Cu_3O_6$.

Shown in Table 6 are the net charges of each Cu and oxygen sites in Cu_3O_{12} and Cu_3O_{10} clusters for $YBa_2Cu_3O_7$ and $YBa_2Cu_3O_6$.

The changes in the formal oxidation state of Cu(1) and Cu(2) for $YBa_2Cu_3O_7$ and $YBa_2Cu_3O_6$ cuprates reasonable

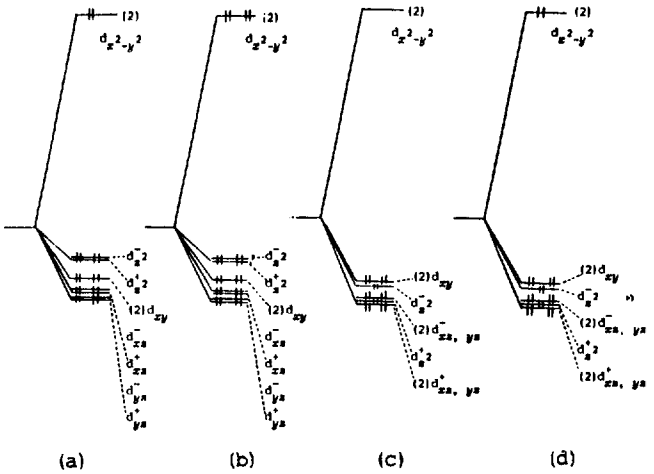

Figure 6-2. The splitting of the *d*-orbitals of Cu(2) by the local crystal field environment: (a) $Cu_3O_{12}^{17-}$; (b) $Cu_3O_{12}^{19-}$; (c) $Cu_3O_{10}^{13-}$; (d) $Cu_3O_{10}^{15-}$ clusters.

Table 4. Valence Electron Population for Cu_3O_{12} and Cu_3O_{10} Clusters

					d component		
		s	*p*	*d*	$d_{x^2-y^2}$	d_{z^2}	t_{2g}
$Cu_3O_{12}^{17-}$	Cu(1)	0.422	0.384	8.586	1.642	0.943	6.000
	Cu(2)	0.386	0.395	9.269	1.317	1.957	5.995
	O(1)	1.937	5.735				
	O(2)	1.937	5.808				
	O(3)	1.944	5.818				
	O(4)	1.903	5.667				
$Cu_3O_{12}^{19-}$	Cu(1)	0.422	0.384	8.586	1.642	0.943	6.000
	Cu(2)	0.387	0.395	9.951	1.999	1.957	5.995
	O(1)	1.937	5.735				
	O(2)	1.940	5.883				
	O(3)	1.947	5.896				
	O(4)	1.903	5.667				
$Cu_3O_{10}^{13-}$	Cu(1)	0.596	0.257	9.784	2.000	1.784	6.000
	Cu(2)	0.395	0.375	8.583	0.634	1.953	5.996
	O(2)	1.936	5.735				
	O(3)	1.936	5.735				
	O(4)	1.891	5.753				
$Cu_3O_{10}^{15-}$	Cu(1)	0.596	0.257	9.785	2.000	1.785	6.000
	Cu(2)	0.395	0.375	9.266	1.317	1.953	5.996
	O(2)	1.940	5.811				
	O(3)	1.940	5.811				
	O(4)	1.891	5.753				

considering the net charges of each Cu ions in Cu_3O_{12} and Cu_3O_{10} clusters as shown in Table 5 are illustrated in Table 7.

Results and Discussion

Electronic structures of the oxygen-deficiency in the $YBa_2Cu_3O_x$ ($6 \leq x \leq 7$) cuprate superconductors are investigated by the extended Hückel molecular orbital (EHMO) theory with tight-binding model. The small clusters $Cu_3O_{12}^{n-}$ as shown in Figure 3(a) and $Cu_3O_{10}^{m-}$ as shown in Figure 3(b)

Table 5. Reduced Overlap Population in Cu_3O_{12} and Cu_3O_{10} Clusters

	Cu(1)–O(4)	Cu(2)–O(4)	Cu(1)–O(1)	Cu(2)–O(2)	Cu(2)–O(3)
$Cu_3O_{12}^{17-}$	0.324	0.064	0.270	0.229	0.206
$Cu_3O_{12}^{19-}$	0.324	0.064	0.270	0.183	0.155
$Cu_3O_{10}^{13-}$	0.360	0.035		0.271	0.271
$Cu_3O_{10}^{15-}$	0.360	0.035		0.222	0.222

Table 6. The Net Charges of each Cu and Oxygen Sites in Cu_3O_{12} and Cu_3O_{10} Clusters

	Cu(1)	Cu(2)	O(1)	O(2)	O(3)	O(4)
$Cu_3O_{12}^{17-}$	1.609	0.951	-1.672	-1.745	-1.762	-1.570
$Cu_3O_{12}^{19-}$	1.609	0.268	-1.672	-1.822	-1.843	-1.570
$Cu_3O_{10}^{13-}$	0.362	1.647		-1.671	-1.671	-1.644
$Cu_3O_{10}^{15-}$	0.362	0.964		-1.750	-1.750	-1.644

Table 7. Formal Oxidation States of Cu(1) and Cu(2) in Cu_3O_{12} and Cu_3O_{10}

	Cu(1)	Cu(2)
$Cu_3O_{12}^{17-}$	3	2
$Cu_3O_{12}^{19-}$	3	1
$Cu_3O_{10}^{13-}$	1	3
$Cu_3O_{10}^{15-}$	1	2

are employed to represent $YBa_2Cu_3O_7$ and $YBa_2Cu_3O_6$, respectively. Here $n = 17$ to 15 and $m = 15$ to 13 when we change the nominal charge of $Cu_3 = +7$ to $+5$.

The total energies, relative stabilities, and energy gaps between Cu(1) $d_{x^2-y^2}$ state and Cu(2) $d_{x^2-y^2}$ state of Cu_3O_{12} and Cu_3O_{10} clusters representing $YBa_2Cu_3O_6$ and $YBa_2Cu_3O_7$ are shown in Table 3. The energy gaps indicate that the antibonding Cu(1) $d_{x^2-y^2}$ MO's in the CuO_3 chain is located significantly higher in energy ($\simeq 0.4$ eV) than the antibonding Cu(2) $d_{x^2-y^2}$ MO's in the CuO_2 layers for Cu_3O_{12} cluster representing $YBa_2Cu_3O_7$, while for Cu_3O_{10} cluster representing $YBa_2Cu_3O_6$ the orbital character of the highest partially (or pairs) occupied MO (HPOMO, or HOMO) and the lowest completely unoccupied MO (LCUMO) of Cu_3O_{12} cluster representing $YBa_2Cu_3O_7$ is reversed and the energy gap is about 1.5 eV.

The orthorhombic $YBa_2Cu_3O_7$ is calculated to be more stable than the tetragonal $YBa_2Cu_3O_6$ and the relative stability decreases gradually with the order of $YBa_2Cu_3O_7$ (+7)→ $YBa_2Cu_3O_7$ (+5)⟶$YBa_2Cu_3O_6$ ($Cu_3 = +7$)⟶$YBa_2Cu_3O_5$ ($Cu_3 = +5$). The gigantic stability difference between two structures results largely from the variation of the local crystal field environment around the Cu(1) in the Cu(1) chain and is a sign of an important implication concerning the role played by the oxygen atoms in the Cu(1) atom plane.

On the basis of the computed *s,p,d* valence populations for Cu and O ions as shown in Table 4 and the net charges as shown in Table 6, we observe that the formal oxidation state of Cu(1) in the CuO_3 chain is +3 and the state of Cu(2) in the CuO_2 layers is +2 in the hypothetical cluster Cu_3O_{12} for $YBa_2Cu_3O_7$ with the nominal charge of $Cu_3 = +7$ as illustrated in Table 7 and is consistent with the Cava *et al.*,[4] Curties *et*

al.,[3] and Whangbo *et al.*[4] More interestingly when we change the nominal charge of $Cu_3 = +7$ to $+5$, the oxidation state of Cu(1) is invariant, but the state Cu(2) varies from $+2$ to $+1$. In the hypothetical cluster Cu_3O_{10} for $YBa_2Cu_3O_6$ the formal oxidation state of Cu(2) is $+3$ when we take the nominal charge of $Cu_3 = +7$, but $+2$ when we change the nominal charge of $Cu_3 = +7$ to $+5$, while the state of Cu(1) is $+1$ independent upon the variation of the nominal charge of $Cu_3 = +7$ to $+5$.

We note that the question of whether oxide oxidation might be favored over formation of $+3$ (or $+1$) oxidation state of Cu(1) cannot really be answered at the level of EHMO used in our cluster calculations. However, the calculated results on the valency of Cu in the clusters Cu_3O_{12} and Cu_3O_{10} for $YBa_2Cu_3O_7$ and $YBa_2Cu_3O_6$ and the formal assignment of charges in these cuprates are in harmony. The net charge for O ions is slightly larger at O(2) and O(3) sites in the CuO_2 layers than at O(1) and O(4) sites near the Cu(1) chain as shown in Table 6. Decomposition of the 3d population shows that the the t_{2g} orbitals are almost full on each Cu site as shown in Table 4. The $d_{x^2-y^2}$ orbitals are partially empty (or are placed by electron pairs) at the Cu(2) with local square pyramidal crystal field environment, while d_{z^2} orbital predominantly contains the partial hole at the Cu(1) with the local square plannar crystal field environment.

The molecular energy levels of $Cu_3O_{12}^{17-}$ for $YBa_2Cu_3O_7$ with the nominal charge of $Cu_3 = +7$ are illustrated in Figure 5(a). Here, in the Cu_3O chain, it is the $d_{z^2-y^2}$ orbital of Cu(1) that plays the main role which the $d_{x^2-y^2}$ orbitals of Cu(2) play in the CuO_2 layers. The Cu(1) $d_{x^2-y^2}$ molecular orbital lies higher in energy than the Cu(2) $d_{x^2-y^2}$ molecular orbitals.

This would be a result[18] of the local square planar crystal field environment of Cu(1) compared to the local square pyramidal crystal field environment of Cu(2), which is a different result to Curtiss, Brun, and Grun's consideration[3] which is caused by the short Cu(1)–O(4) distance compared to the longer Cu(2)–O(3) and Cu(2)–O(2) distances. With two electrons to fill the there upper orbitals of Figure 5(a), the Cu(1) $d_{x^2-y^2}$ MO is empty and the two Cu(2) $d_{x^2-y^2}$ MO's are half-filled, while with four electrons to fill the there upper MO's of Figure 5(b), the Cu(1) $d_{x^2-y^2}$ MO is also empty but the two Cu(2) $d_{x^2-y^2}$ MO's are placed by pairs.

Also a small HOMO–LUMO energy gap (or half-filled energy state) in a small cluster, Cu_3O_{12}, representing the superconducting material $YBa_2Cu_3O_7$ may be interpreted as indication of an onset of metallic character shown in Santoro *et al.*[7]

The molecular energy levels of Cu_3O_{10} cluster for $YBa_2Cu_3O_6$ are illustrated in Figure 5(b), and 5(c). In contrast with the $YBa_2Cu_3O_7$ cuprate superconductor, it is shown that the Cu(1) d_{z^2} molecular orbital lies significantly lower in energy than the Cu(2) $d_{x^2-y^2}$ molecular orbitals of Cu_3O_{10} cluster for $YBa_2Cu_3O_6$ because the local crystal field environment of Cu(1) varies from the square planar crystal field environment to the linear crystal field environment due to the O(1) oxygen-deficiency from the crystal structures of YBa_3O_7.

With two electrons to fill the three upper molecular orbitals shown in Figure 5(c), the Cu(1) d_{z^2} molecular orbital is filled and the twofold degenerate Cu(2) $d_{x^2-y^2}$ state empty. On the other hand, the twofold degenerate Cu(2) $d_{x^2-y^2}$ state are each half-filled in Cu_3O_{10} cluster for $YBa_2Cu_3O_6$ with four electrons to fill as shown in Figure 5(d).

Here the metallic properties may be not found in the former with the nominal charges of $Cu_3 = +7$ as shown in Figure 5(c), while the properties may be found in the latter Cu_3O_{10} cluster for $YBa_2Cu_3O_6$ with the nominal charge of $Cu_3 = +5$ as shown in Figure 5(d).

Another spilitting diagrams of each Cu d-orbitals as shown in Figure 6-1 and 6-2 are more instructive. The variation of the molecular orbital energy levels of Cu(2) in Figure 6-2 are minor between Cu_3O_{12} and Cu_3O_{10} clusters for $YBa_2Cu_3O_7$ and $YBa_2Cu_3O_6$, and this scheme is in agreement with the work of Ihara and others.[16] While the energy schemes of the molecural orbitals of Cu(1) have an important change. This changeover of the schemes of the energy levels may be interpreted as the indication of the different electronic properties between the insulating $YBa_2Cu_3O_6$ and the superconductive $YBa_2Cu_3O_7$.

Particularly, linear electron-hole-electron pair model of $YBa_2Cu_3O_7$ by Whangbo *et al.*[17] describes the Cu(2)–O(4)–Cu(1)–O(4)–Cu(2) linkage by the electron configurations (*i.e.*, Cu^{2+}-$\ddot{O}^{2-}$-Cu^{3+}-$\ddot{O}^{2-}$-$Cu^{2+} \leftrightarrow Cu^{3+}$-$\ddot{O}^{2-}$-$\dot{Cu}^{+}$-$\ddot{O}^{2-}$-$Cu^{3+} \leftrightarrow Cu^{2+}$-$\dot{O}^{-}$-$\dot{Cu}^{+}$-$\dot{O}^{-}$-$Cu^{2+}$). In the present work we see the Cu(2)–O(4)–Cu(1)–O(4)–Cu(2) linkage of $YBa_2Cu_3O_7$ with the nominal oxidation state of $Cu_3 = +7$ to be the linear electron-hole-electron pair model by the electron configuration (*i.e.*, Cu^{2+}-$\ddot{O}^{2-}$-Cu^{3+}-$\ddot{O}^{2-}$-Cu^{2+}). That the oxidation state of Cu (2) is susceptive while the state of Cu(1) is not sensitive to the variation of the nominal state of Cu_3 in both $YBa_2Cu_3O_7$ and $YBa_2Cu_3O_6$ as shown in Table 4 and 6 may be interpreted as indication of the vital role of the local crystal field environment of Cu(1) in $YBa_2Cu_3O_7$ cuprate superconductor.

Shown in Table 5 are reduced overlap populations (ROP) in Cu_3O_{12} and Cu_3O_{10} clusters for $YBa_2Cu_3O_7$ and $YBa_2Cu_3O_6$. Here the ROP of Cu(1)–O(4) is smaller in Cu_3O_{12} cluster for $YBa_2Cu_3O_7$ than in Cu_3O_{10} cluster for $YBa_2Cu_3O_6$, while the ROP of Cu(2)–O(4) is reverse, which represents shortening of Cu(1)–O(4) distance in Cu_3O_{10} cluster for $YBa_2Cu_3O_6$. The ROPs of Cu(1)–O(4) and Cu(2)–O(4) in $YBa_2Cu_3O_6$ independent upon the variation of the nominal charge of Cu_3 are consistent with the same oxidation state of Cu(1) in the Cu(1) chain. The ROPs of Cu(2)–O(2) and Cu(2)–O(3) in Cu_3O_{12} and Cu_3O_{10} clusters for $YBa_2Cu_3O_7$ and $YBa_2Cu_3O_6$ represent the changed formal oxidation state of Cu(2) in the CuO_2 layers.

In conclusion, it is suggested that the local crystal field environment of Cu(1) by the oxygens around the Cu(1) chain may play a vital role in conductivity and superconductivity, either alone or through cooperative electronic coupling with the Cu(2) plane in the $YBa_2Cu_3O_7$ cuprate superconductor.

Acknowledgement. We thank the Korean Council for University Education for the financial support of this work.

References

1. M. K. Mu, J. R. Ashburn, C. J. Torng, P. H. Hor, R. L. Mong, L. J. Huang, Y. Q. Wang, and C. W. Chu, *Phys. Rev. Lett.*, **58**, 908 (1987).
2. R. T. Cava, B. Batalogg, R. B. Van Dover, D. W. Murphy, S. Sunshine, T. Siesrist, T. P. Remeika, E. A. Rietman, S. M. Zahurak, and G. P. Espinosa, *Phys. Rev. Lett.*, **58**, 1676 (1987).
3. L. A. Curtiss, T. O. Brun, and D. M. Gruen, *Inorg. Chem.*, **26**, 1832-1834 (1987).

4. M. H. Whangbo, M. Evain, M. A. Beno, and J. M. Willians, *Inorg. Chem.*, **26**, 1832-1834 (1987).
5. M. A. Beno, L. Soderholm, D. W. Capone, D. G. Hinks, J. D. Jorgensen, I. K. Suhuller, C. U. Segre, K. Z. Hang, and J. D. Grace, *Appl. Phys. Lett.*, **51**, 57 (1987).
6. (a) F. Herman, R. V. Kasowski, and W. Y. Hus, *Phys. Rev.*, **B 36**, 6904 (1987); (b) J. D. Jorgensen, B. W. Veal, W. K. Kwok, G. W. Crabtree, A. Umezawa, L. J. Nowick, and A. P. Paulikas, *Phys. Rev.*, **B 36**, 5731 (1987).
7. A. Santoro, S. Miraglla, and F. Beech, *Mat. Res. Bull.*, **20**, 1007 (1987).
8. (a) F. Beech, S. Miragl, A. Santoro, and R. S. Roth, *Phys. Rev.*, **B 35**, 8778 (1987); (b) M. H. Whangbo, M. Evain, M. A. Beno, U. Geiser, and J. M. Williams, *Inorg. Chem.*, **27**, 467-474 (1988); (c) J. M. Willams, M. A. Beno, K. D. Carlson, U. Geiser, H. C. Ivykano, A. M. Kini, L. C. Poter, A. J. Schultz, R. J. Torm, and H. H. Wang, *Acc. Chem. Res.*, **21**, 1 (1988); (d) C. N. R. Rao, B. Raveau, *Acc. Chem. Res.*, **22**, 106-113 (1989); (e) M. F. Garbauskas, R. W. Green, R. H. Arendt, and J. S. Kasper, *Inorg. Chem.*, **27**, 871 (1988).
9. J. E. Greedan and A. H. O'Reilly, and C. V. Stager, *Phys. Rev.*, **B 35**, 8770 (1987).
10. Y. Lepage, W. R. Mckinnon, J. M. Tarascon, L. H. Greene, G. W. Hull, and D. M. Hwang, *Phys. Rev.*, **B 35**, 7245 (1987).
11. T. Siegrist, S. Stnshine, D. W. Murphy, R. J. Lava, and S. M. Zahurak, *Phys. Rev.*, **B 35**, 7317 (1987).
12. P. M. Grant, R. B. Beyers, E. M. Engler, G. Lim, S. S. Parkim, M. L. Lamirez, V. P. Lee, A. Nazzal, J. E. Vazguez, and R. J. Savoy, *Phys. Rev.*, **B 35**, 7242 (1987).
13. L. F. Matteiss and D. R. Hamann, *T. Solid State Chem.*, **63**, 395 (1987).
14. S. Massida, JaeJun Yu, A. J. Freeman, and D. D. Koelling, *Phys. Lell*, **A 122**, 198 (1987).
15. R. H. Summerville and R. Hoftmann, *J. Am. Chem. Soc.*, **98**, 7240 (1976).
16. H. Ihara, M. Hirahayashi, N. Terada, Y. Kimura, K. Senzaki, M. Akimolo, K. B. Ushida, F. Kawashima, and R. Uzuka, *Jpn. J. Appl. Phys.*, **26**, L 460 (1988).
17. M. H. Whang, E. Canadell, M. Evain, and J. M. Willams, *Inorg. Chem.*, **27**, 2394-2396 (1988).
18. W. R. Lee and K. H. Lee, unpublished work.

Reactions of Thianthrene Cation Radical Perchlorate with N-(p-Methoxyphenyl)benzene- and Methanesulphonamides

Sung Hoon Kim, Jung Hyu Shin, and Kyongtae Kim*

Department of Chemistry, Seoul National University, Seoul 151-742. *Received July 10, 1989*

Reactions of thianthrene cation radical perchlorate (**1**) with N-(*p*-methoxyphenyl)benzenesulphonamide (**14**) in acetonitrile at room temperature afforded various products: thianthrene (**3**), N-(*p*-hydroxyphenyl) benzenesulphonamide (**16**), benzenesulphonamide (**18**), hydroquinone (**20**); 5-(5-benzenesulphonamido-2-methoxyphenyl)-thianthrenium perchlorate(**21**), 2-benzenesulphonamido-2'-hydroxy-5,5'-dimethoxybiphenyl(**24**), 2-benzenesulphonamido-2', 5'-dihydroxy-5-methoxybiphenyl(**25**), and a traceable amount of *p*-quinone(**23**). The formations of part of (**3**) and (**21**) can be explained by either disproportionation or half-regeneration mechanism but those of the remainders by diverse reactions of sulphonamidyl radical (**27**) derived from (**14**) (through single electron transfer, followed by deprotonation processes). Similar results were observed from the reaction with N-(*p*-methoxyphenyl)methanesulphonamide (**15**).

Introduction

Reactions of thianthrene cation radical perchlorate (**1**) with arene- and alkanesulphonamides at room temperature in acetonitrile have shown various aspects, depending on the substituents at nitrogen. That is, reactions with N-free sulphonamides afforded N-sulphonylsulphilimines (**2**) along with thianthrene (**3**) and thianthrene 5-oxide (**4**) after being elapsed with a couple of months[1] (Scheme 1).

Reactions with N-alkylsulphonamides, which were expected to increase the nucleophilic reactivity of amino group due to electron-donating effect of alkyl group, however, did not afford any product containing the sulphonamide moiety even in three months of reaction time. The sulphonamides were almost quantitatively recovered and (**1**) turned to (**3**), (**4**), and thianthreniumylthianthrene perchlorate (**5**)[1] (Scheme 2).

Sulphonamides with N-aryl group reacted smoothly with (**1**) to give 5-(*p*-N-arene- and alkanesulphonamidophenyl)-thianthrenium perchlorate (**6**) in good yields[2] (Scheme 3)

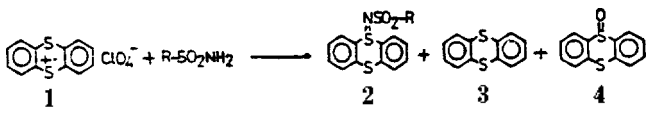

Scheme 1

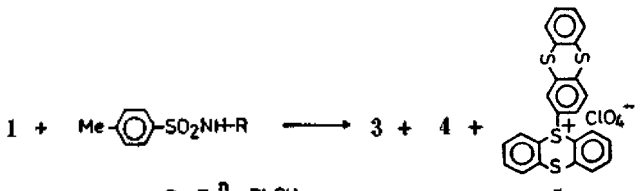

Scheme 2